Transient absorption study on Red Vermilion darkening in presence of chlorine ions and after UV exposure

F.A. Pisu,[1] M. Marceddu,[2] P.C. Ricci,[1] C. Melis,[1] S. Porcu,[1] C.M. Carbonaro,[1] D. Chiriu[1*]

[1] *Dept. of Physics - University of Cagliari, Cittadella Universitaria - S.P. n°8 km 0,700 - 09042 Monserrato CA – Italy*

[2]*CeSAR – University of Cagliari, Cittadella Universitaria - S.P. n°8 km 0,700 - 09042 Monserrato CA – Italy*

[*]*Corresponding Author: daniele.chiriu@dsf.unica.it*

Abstract

The application of no destructive techniques in the field of Cultural Heritage is becoming fundamental to understanding degradation phenomena. In this study, Transient Absorption (TA) spectroscopy was exploited to explain the process which causes the darkening of Red Vermilion, a famous pigment known also as cinnabar. The optical properties involved in the process are studied in pure HgS and chlorine doped HgS samples, before and after exposure to UV light (365 nm). The study was carried out with particular attention on the ground state bleaching signals, directly connected to the formation of intra-gap trap levels responsible for the pigment degradation. First derivative reflectance spectra reveal the presence of these defectivities, while the analysis of Tauc plots from Kubelka Munk function confirms the reduction of energy band gap due to UV exposure. With the help of Density Functional calculations, we simulated the role of S vacancies in producing a defective alpha-phase, the consequent reduction of the energy band gap and, finally, the progressive phase transformation to the cubic metacinnabar. Transient Absorption turns out to be an important tool of diagnosis about the conservation state of pigments applied in the field of Cultural Heritage

Keywords: Vermilion darkening; transient absorption; pump-probe; cinnabar degradation.

1. Introduction

The darkening of red vermilion is the subject of numerous studies engaging the entire community of Cultural Heritage scientists[1–5]. This phenomenon was recently investigated to understand the causes which determine the degradation and the role of other environmental agents in this process[6–9].
Recent works shed light on the possible phase transformation from alpha-cinnabar (red) to beta-cinnabar (black) during the darkening[10–12]. The process is accentuated in presence of halide impurities ions (chlorine) and the formation of metallic Hg was observed. At high concentration the appearance of chlorine-based compounds was not excluded as found in other works[13–17].
Starting from this assumption the aim of this study is oriented to deepen the preliminary analyses proposed in a previous work [18] about the transient absorption properties in pure and Cl-doped HgS samples, both under UV and without exposure conditions.

1.1 Transient Absorption spectroscopy for studying pigments degradation

Pigments degradation is a dynamic phenomenon that affects numerous materials in the field of Cultural Heritage. Several studies analyzed in detail this topic, ranging from structural properties to vibrational fingerprints or colorimetric parameters [19–25]. The color change translates into the variation

of optical characteristics, like absorption, transmittance and reflectance which correlate the electronic properties or band structures with the macro effect on visible rendering.

Transient absorption (TA) spectroscopy is a proficient tool to understand the pigment degradation, because it is able to investigate the changes of the optical properties of a material [26–28]. In this technique, the probe transmittance through the sample is measured both in presence and absence of the pump, as a function of relative time delay between the two pulse. Due to both linear and non-linear interactions, changes in the absorption spectrum of the materials are observed, providing information about the optical interaction, the electronic band structure, excitation and relaxation mechanisms, defects.

There are three main features that can be distinguished in a TA experiment: Ground State Depletion (GSD) or Ground State Bleaching (GSB), Excited State Absorption (ESA) and Stimulated Emission (SE) [29]. In GSD the pump pulse excites the carriers from the ground state to the excited state, thus causing the decrease of the ground state population and the increase of the excited state population. This change of the relative population of the two states lead to a decrease, or bleaching, of the optical absorption, with negative differential absorption spectrum. ESA occurs when the pump photons excite the carriers from the ground state to some excited intermediate state. Subsequent probe photons may excite the carries from this intermediate level to a still higher energy level, thus producing additional new features in the absorption spectrum, with positive differential absorption signatures. Lastly, SE occurs when probe photons stimulate the radiative decay of carriers, previously excited by the probe, leading to the increase of the probe intensity transmitted through the sample, with negative differential absorption.

A deepened analysis of ESA, GSD and SE signals is very useful in studying the position of electronic bands or the presence intermediate levels originating the optical transitions, especially when degradation is appearing.

1.2 Band structure of alpha-HgS, beta-HgS and some Cl-based compounds

Alpha-HgS presents electronic characteristics as a semiconductor with predominant direct transition. Doni et al.[30], studied the band structure of alpha-cinnabar phase reporting in the Brillouin zone a first conduction band at 2.2 eV from the top of the valence band. The energy thickness of the first conduction band is estimated at around 1.5 eV. From the top of the first conduction band, the authors showed a second conduction band located at 1.2 eV. Figure 1A shows a schematic representation of the band structure concerning the phase alpha. In relation to the previous phase, the beta phase exhibits a very short bang gap around 0.25-0.54 eV which characterizes its behaviour similar to metallic Hg. The electronic properties of beta-HgS were studied by Cardona et al. [31] in the Brillouin zone. Instead of the alpha-phase, beta-HgS presents a unique conduction band. We reported in figure 1B a schematic representation of the band structure. For completing the possible scenario of the phase transformation, especially in presence of chlorine impurities, we report also the schematic band structure of calomel (Hg_2Cl_2), corderoite (alpha-$Hg_3S_2Cl_2$) and mercuric chloride ($HgCl_2$) considered in literature the most likely phases that could be formed during the degradation process (figure 1C). Following a recent work of Hogan et al.[3], we report the schematic structure band and the energy gap of these chlorine-based compounds. In particular, for corderoite, calomel and mercuric chloride the energy gap was estimated as 2.90 eV, 3.52 eV and 5.43 eV respectively.

2. Materials and methods

2.1 Materials

2.1.1 Synthetic samples

To deepen the study on the darkening process of vermilion we realized synthetic samples doped with Cl^- with the purpose to study transient absorption properties and simulate the effect of this catalyst agent. Synthetic samples were prepared following our previous work[18], which studied the darkening phenomenon, and proposed a kinetic model of degradation.

Four different concentrations were selected with the intent to cover a wide range of Cl^- ions. We report the assigned nomenclature of samples connected directly to the molar concentration: 0.00M NaCl called "pure"; 0.01M NaCl called "0.01M", 0.1M NaCl called "0.1M" and 5M NaCl called "5M". Solutions were then applied to a specific support to obtain a pigment deposit available for our analysis. All solutions were dropped to glass slides and dried, with the final results of a solid deposit of about 100 μm thickness and covering area of about 2 cm^2.

All synthetic samples were treated under the UV light of a LED at 365 nm (emission with Lorentzian profile having full width half maximum of 10 nm), under constant power density of 10 mW/cm^2, for time ranges between 0 and 200h.

Within the mentioned set of samples, exposed and not exposed to UV light, we selected for this work those which represents the extremes of our region of interest: pure HgS not exposed, pure HgS UV exposed for 148 h, HgS 5M not exposed and HgS 5M UV exposed for 20 h.

To complete the study, we analyzed also for comparison a metallic Hg sample contained between two glass slides.

2.2 Methods

2.2.1 Pump-probe measurements

Transient absorption measurements were performed with a pump-probe differential spectrometer (Ultrafast Systems HELIOS-EOS), with both pump and probe wavelengths generated by a Ti:Sapphire regenerative amplifier (Coherent Libra-F-1K-HE-230), which delivers 100 fs long pulses at 800 nm with 1 KHz repetition rate. The main emission from the regenerative amplifier was splitted into two branches: one sent to an optical parametric amplifier (Light Conversion TOPAS C), in order to generate the pump wavelengths, and the other sent to the sapphire plate of the HELIOS spectrometer, where multicolor probe beam was generated by means of white light supercontinuum generation. The probe pulses were time-delayed with respect to the pump pulses, by passing through a variable digitally controlled optical delay line. The pump and probe beams were then non-collinearly focused and overlapped on the sample surface, with the pump being chopped at 500 Hz, so that half of the transmission spectra were recorded with the pump on, and half with pump off. The Transmission spectra of the probe beam were recorded as a function of the relative delay time, by means of CCD spectrometers and the differential absorption calculated as follows:

$$\Delta A = -\log\left(\frac{\Delta T}{T} + 1\right) = -\log\left(\frac{T_{pump\ on} - T_{pump\ off}}{T_{pump\ off}} + 1\right) \qquad (1)$$

The pump-probe data were obtained varying the pump power in a range between 0.002-0.600 mW and collecting the signal in the "short live" range (10 ps – delay step 0.02 ps) and "long live" range (10 ns – delay step 0.1 ns). We verified that the selected wavelength (400nm) and excitation power did not permanently modifies the optical features of the investigated samples in terms of color variation. On the contrary, we also exploited the 360 nm excitation in the case of pure HgS to show the effects of pump irradiation. At this wavelength we obtained an evident and permanent darkening of the surface.
In the case of metallic Hg the TA signal was recorded in reflectance mode.

2.2.2 Density Functional theory calculations

Quantum-mechanical calculation were performed by means of the Quantum- Espresso package [32] based on density-functional theory (DFT), periodic-boundary conditions, plane-wave basis sets, and pseudo-potentials to represent the ion-electron interactions. The local density approximation (LDA) with the Slater exchange and Perdew-Zunger[33] correlation were used together with PAW pseudopotentials[34,35]. The electronic Kohn Sham wave functions were expanded using a plane wave basis set, up to a kinetic energy cut-off of 29 Ry. Monkhorst-Pack grids were used to sample the Brillouin zone, $4 \times 4 \times 4$-point was used.
The structures were fully relaxed to their equilibrium configuration through the calculation of the forces on atoms and the stress tensor. In the relaxed equilibrium configuration, the forces are less than 0.004 eV/Å and the deviation of the stress tensor from a diagonal hydrostatic form is less than 0.5 kbar.

2.2.3 Reflectance measurements

Reflectance measurements were performed by means of UV–Vis-NIR Agilent Technologies Cary 5000 spectrophotometer equipped with integrating sphere module. The reflection configuration at 10° measures the diffuse reflection of the sample with respect to a reference sample which is considered to have a 100% reflectivity. A calibrated source Illuminant D65 was used to determine the reflectance spectra and for calculating the colorimetric parameters.
Pure and 5 M solutions were dropped and dried upon an inert polyvinyl chloride (PVC) support until a compacted homogenous powder deposit was obtained (disk with r = 16 mm, thickness = 1 mm)

3. Results and discussion

A first result is reported in figure 2 where reflectance spectra of analyzed samples are reported in the range 400-800 nm. These spectra can be correlated directly with the linear absorption by operating a Kubelka-Munk transformation of reported curves. It is worth noting that the first derivatives of reflectance spectra show two weak broad bands at around 650 and 730 nm in exposed samples, suggesting additional absorption properties due to the degradation process. No other additional bands are evidenced especially in the region before 600 nm which represents the fundamental transition. These information are useful in the interpretation of transient absorption spectra.

Figure 3 reports the spectrograms of unexposed and exposed pure HgS sample. The false color scale of the spectrograms shows a differential absorption signal measured in optical density (OD) ranging from positive (red color) to negative (blue color) values. TA spectra and decay profiles can be extracted from the maps by integrating the signal upon specific time and wavelength range, respectively. Those spectra and profiles are reported on top and on the right of each spectrogram. Reported data are perfectly reproducible for each point of analysis and are completely representative of these samples.

Unexposed pure sample presents a short positive signal at 784 and 806 nm followed by a long signal after the first 2.5 ps (figure 3A). Contextually, the sample shows a short negative signal at 670 nm closed after 6 ps and a combined signal at around 480 nm with an initial short negative contribution of around 1 ps which converts to a positive signal of about 10 ps. Figure 3A and 3B presents the time profile of mentioned signals. Positive signals were revealed over a pump power threshold of 200 μW.

A different trend can be evidenced for the exposed pure sample after 148h of UV irradiation, where a short negative signal centered at 630 nm, converts within 3 ps into a composite positive signal with two bands at 530 nm and 650 nm. These positive signals present a "long-lived" time (see figure 3C). In addition, the UV irradiated sample shows other two long signals in the ns region, not observed in the pure sample: a negative contribution between 650 nm (broad band) and 800 nm (narrow band) and a positive one picked at 480 nm. Both signals have a decay time of around 5 ns. Figure 3D summarizes the spectra of the mentioned long signals and their temporal evolution. Finally, figure 3E shows the additional UV induced negative signals at 740 and 770 nm obtained by using 40 mW of the 360 nm line as pump.

Regarding the samples doped with Cl- ions, we found a sort of variability of the signal depending on the sampled point. This reproducibility calls for a non-uniform effect of Cl doping on the samples, as the grained morphology of the samples (see ref. 18) could also suggest. Despite these variations, the results can be reconducted to few trends that mainly appear in the sampled points. We summarize in figure 4 the main features of TA collected in these points.

Unexposed doped sample exhibits a long positive signal at 490nm, a short negative signal at 670 nm which becomes positive after 2 ps, while a double positive signal at 530 and 660 nm with time decay around 30 ps was delineated. In addition, short negative signals at around 770 and 810 nm can be evidenced for this sample. All the mentioned results are reported in figure 4A-C. For exposed doped sample, the interaction with UV light for 20 h reveals a positive double signal similar to the one discussed for the not irradiated sample, peaked at the same wavelengths, but with reduced decay time of 15 ps (figure 4D). At low pump power (50 μW) the sample shows short negative signals at 740 nm and 795nm which end after 6 ps. Under the same low pump power condition, a very short positive signal is observed at 776 nm (figure 4E).

The relevant variation with respect to the unexposed samples, observed also in pure series, is the presence of long signals, positive and negative, in the range of ns. In particular, we observed a positive signal at 480 nm with a decay time of around 1 ns and a negative signal at 797 nm with a decay time of 3 ns. We reported these results in figure 4F.

Finally, to have an exhaustive panorama of the samples, in comparison with the results proposed in our previous work, we analyzed by pump-probe measurement a metallic Hg sample whose results are reported in figure 5. This sample presents a fingerprinting long negative signal in the range of ns between 450 and 800 nm.

3.1 Assignations

By taking into account the photon energies associated to the pump and probe wavelengths, and the linear absorption properties discussed in figure 2, we tried to correlate the positive and negative TA signals to the band structure delineated before. In particular, as depicted in figure 6, the positive signal at 480 nm (2.58 eV) is compatible with an Excited State Absorption (ESA) which promotes an electron to an excited state located in the first conduction band (I C.B.), after pump absorption, and consequently a transition to the second conduction band (II C.B.) when the probe photons are absorbed. Analogously, the 800 nm (1.54 eV) positive signal is consistent with an ESA in which a metastable level is located in the prohibited band between the first and second conduction bands. For what concerns the negative signal, a Ground State Depletion (GSD) can be associated to the negative band at 670-680 nm (1.82 eV)

compatible with the presence of intragap levels saturating after the absorption of the probe. In terms of structural properties, the mentioned GSD signal is in accord with the formation of intrinsic defects corresponding to shallow trap levels in the first prohibited region. The same typology of GSD is confirmed at 670-680 nm in the exposed pure sample with the addition of a broadening toward the lower energies up to 800 nm. The UV treatment produces also other defects revealed by a "long-lived" GSD signal at 800 nm (1.54 eV) found only in UV treated samples. These defects cause the presence of deep traps from the bottom of the first conduction band which corresponds to a consistent darkening effect in the visible region. The formation of defects is further confirmed by the irradiation with the pump at 360 nm, as recorded in Fig. 3E. Moreover, the application of UV light to the samples changes drastically the characteristic decay time of the revealed signals that moved in the ns range. In particular, a long ESA is revealed at 480 nm and a long bleaching at around 800 nm. The latter assumes a very similar trend as compared to metallic Hg which presents a "long-lived" negative signal for all the explored wavelengths (figure 5). The reported results suggest the formation of a cinnabar phase upon UV irradiation with spectral features similar to metallic Hg. Concerning the attribution of this phase and in particular the detection of the beta-cinnabar phase, it is worth noting that in the investigated spectral region it would be impossible to distinguish between beta-cinnabar phase and metallic Hg. Indeed, according to the band structure sketched in figure 1, the band gap of the black beta phase is around 0.25-0.54 eV which corresponds to the 2200nm-5000nm IR region. This range is out of our experimental setup and, by using the presented pump-probe configuration, it is impossible for us to distinguish between metallic Hg and beta phase. However, as illustrated before, the presence of defectivities producing a band gap reduction, and consequently a darkening effect, lead us to suppose a progressive formation of a strongly defective alpha phase. We expect that when the number of defects is structurally unsustainable for this configuration, the alpha phase transforms to beta one, as proved in [10].

Concerning the presence of chlorine ions, they seem to not change the structure of the alpha-phase, since only small variations in the GSD spectra and characteristic decay times are revealed. In particular, figures 4C and 4E show well-defined negative bands between 700 and 800 nm which can be ascribed to the presence of further trap centers due to the Cl^- ions in the structure. Even the UV treatment does not display an evident difference between doped and undoped samples, except for a shortening of characteristic decay times of involved transitions. Most important, all the transitions involved in pump–probe measurement do not appear as compatible with the formation of other chlorine-based phases like calomel or mercury chloride which present a higher band gap than pure cinnabar. Only the corderoite phase could have a possible matching since its band gap at 2.90 eV is compatible with the revealed ESA signals, but in that case the formation of deep traps at 1.82 eV and 1.54 eV could hardly explain the observed darkening phenomena and the recorded changes in the kinetics of the absorption features.

Following the just proposed comments, we calculated the band gap for the experimental samples starting from the Reflectance spectrum and by elaborating the Tauc plots for Kubelka Munk function [36][37] expressed in equation 2:

$$F(R) = \frac{(1-R)^2}{2R} \quad (2)$$

Figure 7 displays the results obtained in samples before and after the UV treatment, evidencing the transition to a phase with a reduced gap. In particular, we reported in the figure the direct and indirect transitions for all the samples that are summarized in Table I. Upon UV irradiation, pure HgS transitions move from 2.05 eV to 1.92 eV for direct transitions and from 1.97 eV to 1.57 eV for indirect transitions. The HgS 5M sample changes the transitions from 2.08 eV to 2.01 eV (direct) and from 1.93 eV to 1.77 eV (indirect). These values are compatible with GSD signals obtained by pump-probe and a similar trend

evidenced in the first derivative reflectance spectrum (figure 8), where two satellite broad bands are indicated at 650 nm and 740 nm. We underline that the presence of indirect transitions justifies the time extension of pump-probe signal from picoseconds to the nanosecond regime. Actually, as suggested by several authors[38–40], a phonon assisted recombination for these indirect transitions influences the time of the entire process, especially the absorption of free carriers. Indeed, as studied by Cooper et al. [27], the change of differential absorption coefficient dα is a function of both photon energy and time (Eq. 3):

$$\mathrm{d}\alpha(E,t) = \frac{4\pi}{\lambda}(\mathrm{d}\kappa_{\Delta E_g} + \mathrm{d}\kappa_{\Gamma} + \kappa_{\mathrm{Drude}}) \qquad (3)$$

As evidenced in equation 2, the change of the extinction coefficient depends on the shifting of the band gap ($\mathrm{d}\kappa_{\Delta \mathrm{Eg}}$), broadening of the band gap ($\mathrm{d}\kappa_{\Gamma}$), and Drude-like free-carrier absorption (κ_{Drude}) components. This equation is related to the experimental differential optical density (dOD) through the Beer-Lambert law. In particular, following the recent study of Cooper, the time dependence of dOD can be determined by the sum of two terms:

$$\mathrm{d}OD(\lambda,t) = \mathrm{d}OD(t) + Q(t)\mathrm{d}OD_{thermal} \qquad (3)$$

which represent, respectively, the contribution of above-mentioned extinction coefficient parameters and a time-dependent weighted function (Q(t)) of thermal contributions. Cooper hypothesized that the temporal evolution in the picosecond regime is dominated by a relaxation of hot photo-excited carriers which occurs primarily through carrier/carrier scattering. Conversely, carrier/lattice scattering and consequent dissipation to lattice heating occur in a second time up to the nanoseconds regime.
This trend is consistent with our experimental results and could explain the change of time range associated to the band gap reduction causing the darkening macro effect. In addition, the carrier/lattice scattering is favorable in the transition to quasi metal (beta phase) or metal nature (metallic Hg), where phonon assisted recombination and lattice heating occur efficiently.
The role of chlorine ions in HgS deserves a brief discussion in order to summarize the effects produced in the process. In terms of TA, chlorine ions do not cause a particular effect in ESA or GSD signals in samples without UV exposure. For what concerns the doped sample after UV irradiation we evidenced a lower threshold for short GSD and a higher threshold for long GSD and ESA signals. The spectral positions of intermediate states which origin the optical transition seem not to change with the presence of chlorine ions. To conclude our analysis, Tauc plots confirm the presence of alpha-cinnabar with a defective phase, but the formation of other chlorine-based compounds having a band gap over 2.0 eV seems to be ruled out, since all the mentioned possible Cl related structures, corderoite, calomel and mercury chloride, are endowed with higher values of band gap.

To gather further information a detailed study of TA signals and characteristic times as a function of injection fluence derived from pump power is proposed in the Supplementary Materials (figure S1 and S2). In particular, at low fluence, the GSD is the most predominant phenomenon. In this process, a fraction of carriers' number is promoted in the excited state, while the carriers' amount in the ground state decreases leading to a negative signal of TA. In the first fluence range, signal intensities and characteristic times follow a linear trend as a function of pump power, while as the laser fluence increases we observed a saturation of these observables and, in some cases, an inversion in the trend. This phenomenon is well known in literature [41]: at higher laser fluences, the third-order nonlinear effects such as absorption saturation, exciton−exciton annihilation, Auger processes, and excited-state absorption are prominent. During such nonlinear excitation phenomena, the excited states may get fully filled (near full bleach of the ground state) leading to TA signal saturation and even a trend inversion.

Indeed, the GSD lifetimes in the present case show a decreasing trend with an increase of laser fluence, which further suggests the involvement of third-order nonlinear effects. Concerning the ESA signal, we analyzed in detail the 480nm transition in unexposed pure sample (see figure S3). In this case a nonlinear scaling with pump power is recorded, with a threshold around 200 μW (fluence of 70 μJ/cm^2), further confirming the involvement of non-linear processes. In addition, a hysteresis of the signal is evident, and it could be associated to possible permanent changes once the threshold is reached.

3.2 Density Functional Theory calculations

In order to shed light on the nature of the experimentally observed traps, and with the intention to confirm the phase transition, we performed a DFT calculation starting from literature and following our previous work where the S vacancies led to an excess of Hg [18].

The initial structure of Alpha-HgS, obtained from single crystal data, was fully optimized to the equilibrium positions and the supercell containing 48 atoms was relaxed to a target pressure smaller than 0.5 kbar. The corresponding optimized lattice parameters *a* and *c* were found to be respectively *a*= 4.225 Å and *c*=9.7678 Å which agree to better than 3% with the experimental values of *a* = 4.15 Å and *c* = 9.5 Å[6,42].

Starting from the Alpha-HgS optimized structure, we estimated the corresponding band structures by means of the Quantum-espressso package. The calculations show an indirect energy gap of 0.93 eV which is considerably smaller than the corresponding experimentally gap of 2.25 eV[43]. The energy gap underestimation is a well-known DFT problem which appears when local density functionals are used in the calculations.

In order to characterize the effects of point defects on the alpha-HgS optical properties, we performed a series of band-structure calculations on alpha-HgS having an increasing density of S vacancy in the range 6.5 x 10^{20}- 4.9 x 10^{21} cm^{-3}.

Figure 8A shows the alpha-HgS energy gap as a function of the vacancy concentration. We observe an overall non-monotonic energy-gap (EG) in relation to the number of vacancies (NV). For NV up to ~6.5x10^{20} cm^{-3} the EG does not significantly change with respect to pristine alpha-HgS. On the other hand, by increasing NV in the range 1-2 x 10^{21} cm^{-3}, we observe a significant EG reduction down to ~0.25 eV, suggesting a possible transition to the beta-phase. We attribute such an energy gap reduction to the occurrence of spurious vacancy energy levels within the energy band gap. This hypothesis is confirmed in Fig. 8B, where the electronic density of states is plotted for pristine HgS and for NV=1x10^{21} cm^{-3}. The inset clearly indicates the presence of energy vacancy levels positioned within the energy gap which is therefore reduced down to a value of ~0.25 eV. Finally, for NV=4x10^{21} cm^{-3}, we observe an unexpected EG increase up to ~1.1 eV. However, by analyzing the corresponding HgS structure we observe an overall lack of hexagonal crystallinity being the system mostly amorphous.

4. Conclusions

Transient absorption on pure HgS and chlorine doped HgS was used to characterize the optical properties of Red Vermilion in relation to the darkening effect. The results were compared with those obtained in samples exposed to UV light which presented evident blackening of their original color. Pump probe measurements reveal positive and negative signals ascribed to a broad short GSD at 680 nm and ESA at 480-500 nm. The former is attributed to the presence of traps (0.2 eV from the bottom of the first conduction band) in a "defective" phase, the latter to transitions from the first to the second conduction band. In particular, with the intention to explain the darkening phenomenon, the GSD signals were also studied in UV exposed samples which reveal, beyond the short GSD, the presence of long a GSD at 780-

800 nm compatible with a phonon-assisted transition. This behavior is compatible with indirect transitions which explain the reduction of the band gap and reflect the darkening process. Actually, for UV exposed samples the analysis of Tauc plots from Kubelka Munk function of reflectance spectra reveals a band gap change from around 2.0 eV to 1.57 eV for pure HgS and from around 2.0 eV to 1.77 eV for 5M HgS. The results are in agreement with DFT simulations that show a progressive reduction of the energy gap as a function of S vacancies in the cell. The formation of intra-gap defect levels is also confirmed. These important conclusions confirm our previous results, obtained with the use of Raman spectroscopy, where a kinetic model of phase transition from cinnabar to beta-cinnabar and metallic Hg was proposed. In addition, the combined use of transient absorption and reflectance measurements could be considered an important tool to understand the degradation phenomena and diagnose the conservation state of pigments applied in the field of Cultural Heritage.

Author contributions

D.C. supervised the project, performed all experiments, analyzed and interpreted the data.; F.A.P. prepared the synthetic samples, performed the experiments regarding the synthetic samples and analyzed the data; S. P., P.C.R., M.M. and C.M.C. performed all experiments and participated in data interpretation. C.M. performed DFT simulations and participated in data interpretation.

Declaration of competing interest

The authors declare that they have no known competing financial interests or personal relationships that could have appeared to influence the work reported in this paper.

Acknowledgments: All the authors acknowledge the CeSAR (Centro Servizi Ricerca d'Ateneo) core facility of the University of Cagliari for assistance with the generation of transient absorption data.

References

[1] Elert K, Cardell C. Weathering behavior of cinnabar-based tempera paints upon natural and accelerated aging. Spectrochim Acta - Part A Mol Biomol Spectrosc 2019. https://doi.org/10.1016/j.saa.2019.03.027.

[2] Radepont M, Coquinot Y, Janssens K, Ezrati JJ, De Nolf W, Cotte M. Thermodynamic and experimental study of the degradation of the red pigment mercury sulfide. J Anal At Spectrom 2015. https://doi.org/10.1039/c4ja00372a.

[3] Hogan C, Da Pieve F. Colour degradation of artworks: An ab initio approach to X-ray, electronic and optical spectroscopy analyses of vermilion photodarkening. J Anal At Spectrom 2015. https://doi.org/10.1039/c4ja00327f.

[4] Gettens RJ, Feller RL, Chase WT. Vermilion and cinnabar. Stud Conserv 1972. https://doi.org/10.1179/sic.1972.006.

[5] Radepont M. Understanding of chemical reactions involved in pigment discoloration, in particular in mercury sulfide (HgS) blackening. Anal Chem 2013.

[6] Ballirano P, Botticelli M, Maras A. Thermal behaviour of cinnabar, α-HgS, and the kinetics of the β-HgS (metacinnabar) - α-HgS conversion at room temperature. Eur J Mineral 2014. https://doi.org/10.1127/0935-1221/2013/0025-2341.

[7] Feller RL. Studies on the darkening of vermilion by light. Rep Stud Hist Art 1967.

[8] Keune K, Boon JJ. Analytical imaging studies clarifying the process of the darkening of vermilion in paintings. Anal Chem 2005. https://doi.org/10.1021/ac048158f.

[9] Duan X, Li X. Exploring the influence of water molecules on the stability of the cinnabar oxides. Chem Phys Lett 2020. https://doi.org/10.1016/j.cplett.2020.137351.

[10] Yu J, Warren WS, Fischer MC. Visualization of vermilion degradation using pump-probe microscopy. Sci Adv 2019. https://doi.org/10.1126/sciadv.aaw3136.

[11] Daniels V. The blackening of vermilion by light. Recent Adv. Conserv. Anal. artifacts Jubil. Conserv. Conf. Pap. London 6-10 July 1987, 1987.

[12] Spring M, Grout R. The Blackening of Vermilion: An Analytical Study of the Process in Paintings Introduction. Natl Gall Tech Bull 2002. https://doi.org/10.1002/col.5080050319.

[13] McCormack JK. The darkening of cinnabar in sunlight. Miner Depos 2000. https://doi.org/10.1007/s001260050281.

[14] Da Pieve F, Hogan C, Lamoen D, Verbeeck J, Vanmeert F, Radepont M, et al. Casting light on the darkening of colors in historical paintings. Phys Rev Lett 2013. https://doi.org/10.1103/PhysRevLett.111.208302.

[15] Cotte M, Susini J, Metrich N, Moscato A, Gratziu C, Bertagnini A, et al. Blackening of Pompeian cinnabar paintings: X-ray microspectroscopy analysis. Anal Chem 2006. https://doi.org/10.1021/ac0612224.

[16] Neiman MK, Balonis M, Kakoulli I. Cinnabar alteration in archaeological wall paintings: an experimental and theoretical approach. Appl Phys A Mater Sci Process 2015. https://doi.org/10.1007/s00339-015-9456-x.

[17] Radepont M, De Nolf W, Janssens K, Van Der Snickt G, Coquinot Y, Klaassen L, et al. The use of microscopic X-ray diffraction for the study of HgS and its degradation products corderoite (α-Hg3S2Cl 2), kenhsuite (γ-Hg3S2Cl2) and calomel (Hg2Cl2) in historical paintings. J Anal At Spectrom 2011. https://doi.org/10.1039/c0ja00260g.

[18] Chiriu D, Pala M, Pisu FA, Cappellini G, Ricci PC, Carbonaro CM. Time through colors: A kinetic model of red vermilion darkening from Raman spectra. Dye Pigment 2021. https://doi.org/10.1016/j.dyepig.2020.108866.

[19] Pisu FA, Chiriu D, Ricci PC, Carbonaro CM. Defect Related Emission in Calcium Hydroxide: The Controversial Band at 780 cm−1. Crystals 2020. https://doi.org/10.3390/cryst10040266.

[20] Pisu FA, Carbonaro CM, Corpino R, Ricci PC, Chiriu D. Fresco paintings: Development of an aging model from 1064 nm excited raman spectra. Crystals 2021. https://doi.org/10.3390/cryst11030257.
[21] Gueli AM, Bonfiglio G, Pasquale S, Troja SO. Effect of particle size on pigments colour. Color Res Appl 2017. https://doi.org/10.1002/col.22062.
[22] Harrison J, Lee J, Ormsby B, Payne DJ. The influence of light and relative humidity on the formation of epsomite in cadmium yellow and French ultramarine modern oil paints. Herit Sci 2021. https://doi.org/10.1186/s40494-021-00569-2.
[23] Rosi F, Grazia C, Gabrieli F, Romani A, Paolantoni M, Vivani R, et al. UV–Vis-NIR and micro Raman spectroscopies for the non destructive identification of Cd 1−x Zn x S solid solutions in cadmium yellow pigments. Microchem J 2016;124:856–67. https://doi.org/10.1016/j.microc.2015.07.025.
[24] Comelli D, Maclennan D, Ghirardello M, Phenix A, Schmidt Patterson C, Khanjian H, et al. Degradation of Cadmium Yellow Paint: New Evidence from Photoluminescence Studies of Trap States in Picasso's Femme (époque des "demoiselles d'Avignon"). Anal Chem 2019. https://doi.org/10.1021/acs.analchem.8b04914.
[25] Chiriu D, Ricci PC, Carbonaro CM, Nadali D, Polcaro A, Collins P. Raman identification of cuneiform tablet pigments: emphasis and colour technology in ancient Mesopotamian mid-third millennium. Heliyon 2017;3:e00272. https://doi.org/10.1016/j.heliyon.2017.e00272.
[26] Fischer MC, Wilson JW, Robles FE, Warren WS. Invited Review Article: Pump-probe microscopy. Rev Sci Instrum 2016. https://doi.org/10.1063/1.4943211.
[27] Cooper JK, Reyes-Lillo SE, Hess LH, Jiang CM, Neaton JB, Sharp ID. Physical Origins of the Transient Absorption Spectra and Dynamics in Thin-Film Semiconductors: The Case of BiVO4. J Phys Chem C 2018. https://doi.org/10.1021/acs.jpcc.8b06645.
[28] Berera R, van Grondelle R, Kennis JTM. Ultrafast transient absorption spectroscopy: Principles and application to photosynthetic systems. Photosynth Res 2009. https://doi.org/10.1007/s11120-009-9454-y.
[29] Garmire EM. Photonics: Linear and Nonlinear Interactions of Laser Light and MatterPhotonics: Linear and Nonlinear Interactions of Laser Light and Matter , Ralf Menzel Springer-Verlag, New York, 2001. $89.95 (873 pp.). ISBN 3-540-67074-2 . Phys Today 2002. https://doi.org/10.1063/1.1472399.
[30] Doni E, Resca L, Rodriguez S, Becker WM. Electronic energy levels of cinnabar (-HgS). Phys Rev B 1979. https://doi.org/10.1103/PhysRevB.20.1663.
[31] Cardona M, Kremer RK, Lauck R, Siegle G, Muñoz A, Romero AH. Electronic, vibrational, and thermodynamic properties of metacinnabar β-HgS, HgSe, and HgTe. Phys Rev B - Condens Matter Mater Phys 2009. https://doi.org/10.1103/PhysRevB.80.195204.
[32] Giannozzi P, Baroni S, Bonini N, Calandra M, Car R, Cavazzoni C, et al. QUANTUM ESPRESSO: A modular and open-source software project for quantum simulations of materials. J Phys Condens Matter 2009. https://doi.org/10.1088/0953-8984/21/39/395502.
[33] Perdew JP, Zunger A. Self-interaction correction to density-functional approximations for many-electron systems. Phys Rev B 1981. https://doi.org/10.1103/PhysRevB.23.5048.
[34] Kresse G, Furthmüller J. Efficient iterative schemes for ab initio total-energy calculations using a plane-wave basis set. Phys Rev B - Condens Matter Mater Phys 1996. https://doi.org/10.1103/PhysRevB.54.11169.
[35] Blöchl PE. Projector augmented-wave method. Phys Rev B 1994. https://doi.org/10.1103/PhysRevB.50.17953.
[36] Jubu PR, Yam FK, Igba VM, Beh KP. Tauc-plot scale and extrapolation effect on bandgap estimation from UV–vis–NIR data – A case study of β-Ga2O3. J Solid State Chem 2020.

https://doi.org/10.1016/j.jssc.2020.121576.
[37] Tauc J, Grigorovici R, Vancu A. Optical Properties and Electronic Structure of Amorphous Germanium. Phys Status Solidi 1966. https://doi.org/10.1002/pssb.19660150224.
[38] Kumar S, Khorasaninejad M, Adachi MM, Karim KS, Saini SS, Sood AK. Probing ultrafast carrier dynamics, nonlinear absorption and refraction in core-shell silicon nanowires. Pramana - J Phys 2012. https://doi.org/10.1007/s12043-012-0337-y.
[39] Knowles KE, Koch MD, Shelton JL. Three applications of ultrafast transient absorption spectroscopy of semiconductor thin films: Spectroelectrochemistry, microscopy, and identification of thermal contributions. J Mater Chem C 2018. https://doi.org/10.1039/c8tc02977f.
[40] Ravensbergen J, Abdi FF, Van Santen JH, Frese RN, Dam B, Van De Krol R, et al. Unraveling the carrier dynamics of BiVO4: A femtosecond to microsecond transient absorption study. J Phys Chem C 2014. https://doi.org/10.1021/jp509930s.
[41] Adnan M, Prakash GV. Study of Surface and Bulk Recombination Kinetics of Two-Dimensional Inorganic-Organic Hybrid Semiconductors under Linear and Nonlinear Femtosecond Transient Absorption Analysis. J Phys Chem C 2021;125:12166–74. https://doi.org/10.1021/acs.jpcc.1c02351.
[42] T. Schleid, P. Lauxmann and CS. Special Issue. Z Krist 1999:95.
[43] Zallen R. II-VI Semiconducting Compounds. NY: 1967.
[44] Sznajder M, Bercha DM, Kharkhalis LY. The band structure of a layered Hg3TeCl4 crystal formed by energy states of HgCl2 and HgTe crystals. Phys Status Solidi Basic Res 2008. https://doi.org/10.1002/pssb.200743532.
[45] Pelant I., Popova M. N., Hàla J., Ambroz M., Lhotskà V. VK. TWO-PHOTON ABSORPTION AND ENERGY BAND STRUCTURE OF ORTHORHOMBIC Hg2C12 CRYSTALS. Czech J Phys B37 1987:1183.

Figures and Tables

Figure 1: Sketch of band structure of HgS phases and some compounds correlated to cinnabar darkening: alpha-HgS (A); beta-HgS (B); alpha-$Hg_3S_2Cl_2$ [3](C); $HgCl_2$[44] (D), Hg_2Cl_2 [45] (D).

Figure 2: Reflectance (A) and first derivative Reflectance (B) spectra in the range 400-800 nm.

Figure 3: Transient absorption maps, wavelength and time profiles of HgS pure samples: unexposed sample in the range 750-810nm (A); unexposed complete range (B); exposed (C); exposed observed in long-time range (D); UV induced dark in unexposed sample through 40 mW of 360 nm line excitation (E).

Figure 4: Transient absorption maps, wavelength and time profiles of 5M doped samples: unexposed point 1(A); unexposed point 2(B); unexposed point 3 (C); exposed point 1(D); exposed point 2 (E); exposed observed in long-time range (F).

Figure 5: Transient absorption map, wavelength and time profiles of metallic Hg.

Figure 6: Reconstruction of darkening process in the band structure sketches of HgS phases by means of ESA and GSD transitions from TA maps: presence of ESA in alfa-HgS (A); addition of shallow traps in intrinsic defective alpha-HgS (B); UV induced defects in alpha-HgS (C); metallic behaviour of beta-HgS and metallic Hg (D).

Figure 7: Tauc Plots for Kubelka Munk function from Reflectance spectra of analyzed samples: direct and indirect transitions for pure and doped samples not exposed to UV light (A); direct and indirect transitions for UV exposed pure and doped samples (B);

Figure 8: DFT calculation of energy gap of alpha-HgS as a function of S vacancies in the structure (A); Electronic density of states for pristine HgS and number of vacancies NV=$1x10^{21}$ cm^{-3} (B).

Table I: resume of direct and indirect transitions for all the samples calculated from figure 7 before and after UV exposure.

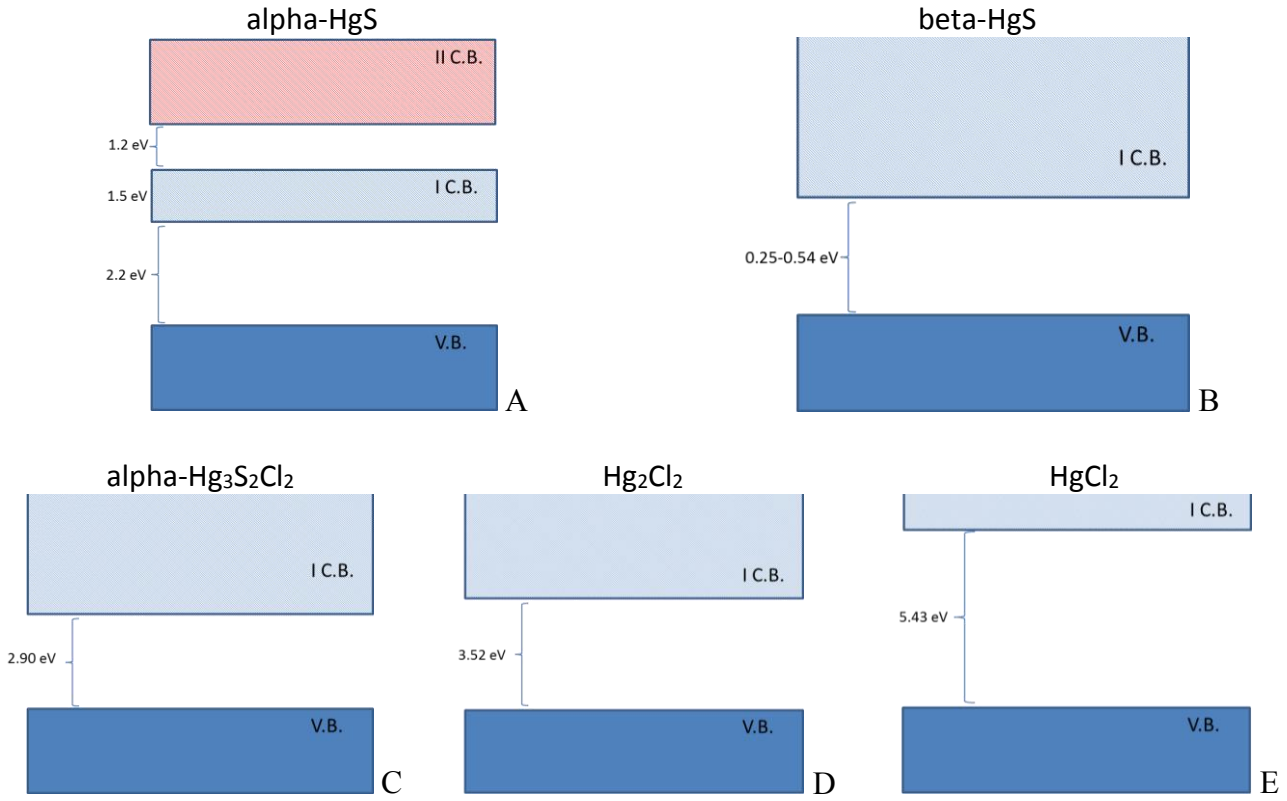
alpha-HgS
II C.B.
1.2 eV
1.5 eV
I C.B.
2.2 eV
V.B.
A
beta-HgS
I C.B.
0.25-0.54 eV
V.B.
B
alpha-Hg3S2Cl2
I C.B.
2.90 eV
V.B.
C
Hg2Cl2
I C.B.
3.52 eV
V.B.
D
HgCl2
I C.B.
5.43 eV
V.B.
E

Figure 1

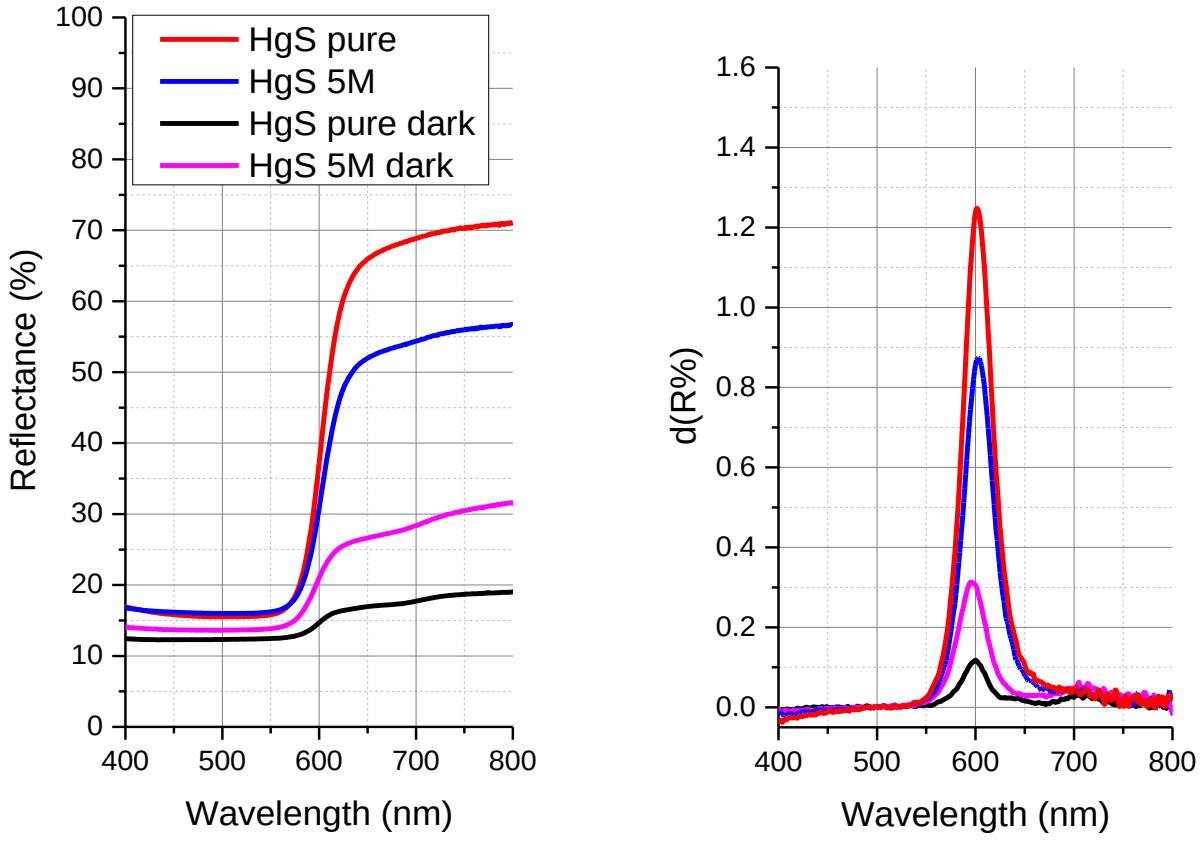

A B

576 Figure 2

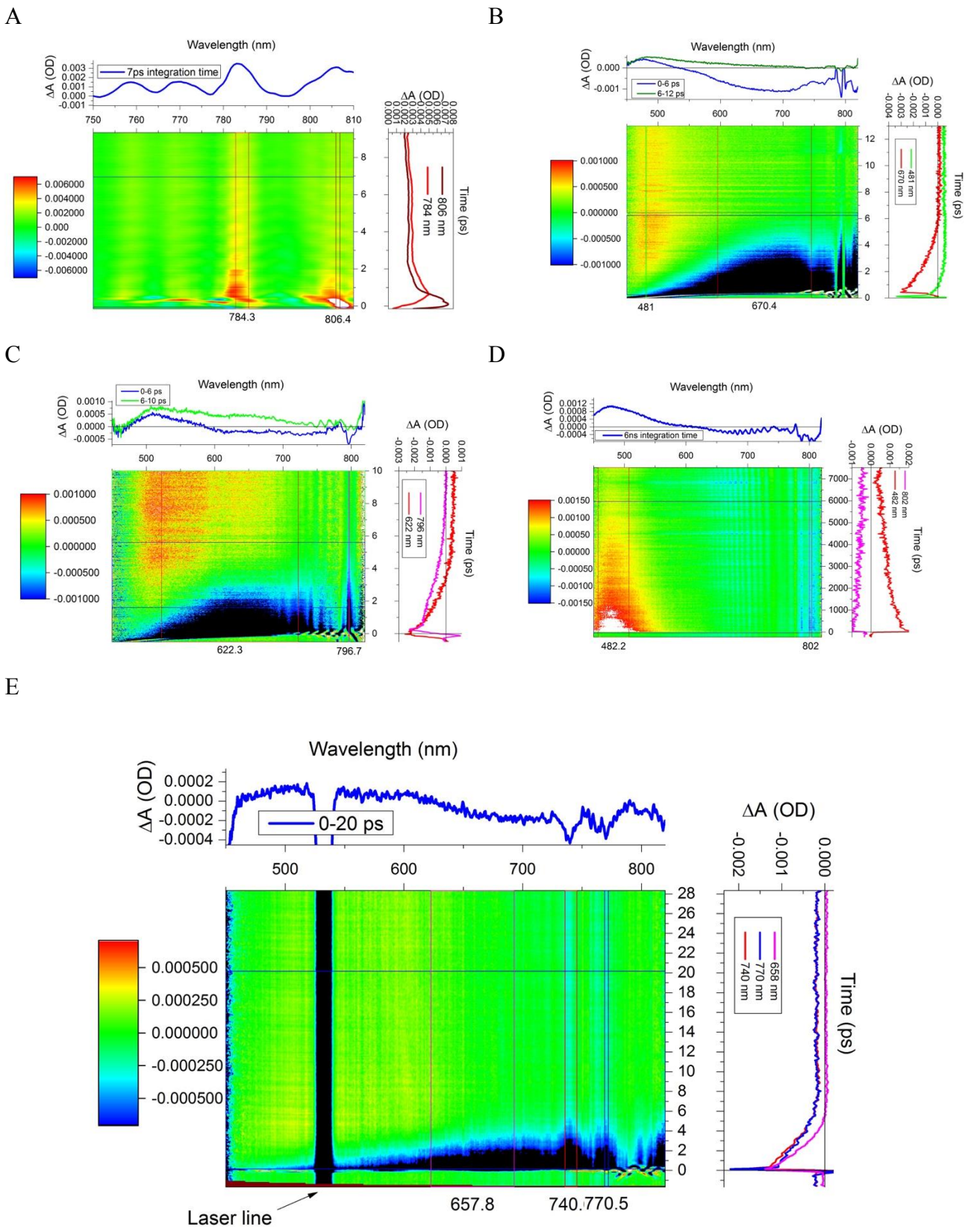
A
Wavelength (nm)
ΔA (OD)
7ps integration time
ΔA (OD)
806 nm
784 nm
Time (ps)
784.3
806.4
B
Wavelength (nm)
ΔA (OD)
0-6 ps
6-12 ps
ΔA (OD)
481 nm
670 nm
Time (ps)
481
670.4
C
Wavelength (nm)
ΔA (OD)
0-6 ps
6-10 ps
ΔA (OD)
796 nm
622 nm
Time (ps)
622.3
796.7
D
Wavelength (nm)
ΔA (OD)
6ns integration time
ΔA (OD)
802 nm
482 nm
Time (ps)
482.2
802
E
Wavelength (nm)
ΔA (OD)
0-20 ps
ΔA (OD)
658 nm
770 nm
740 nm
Time (ps)
Laser line
657.8
740.770.5

577 Figure 3

578

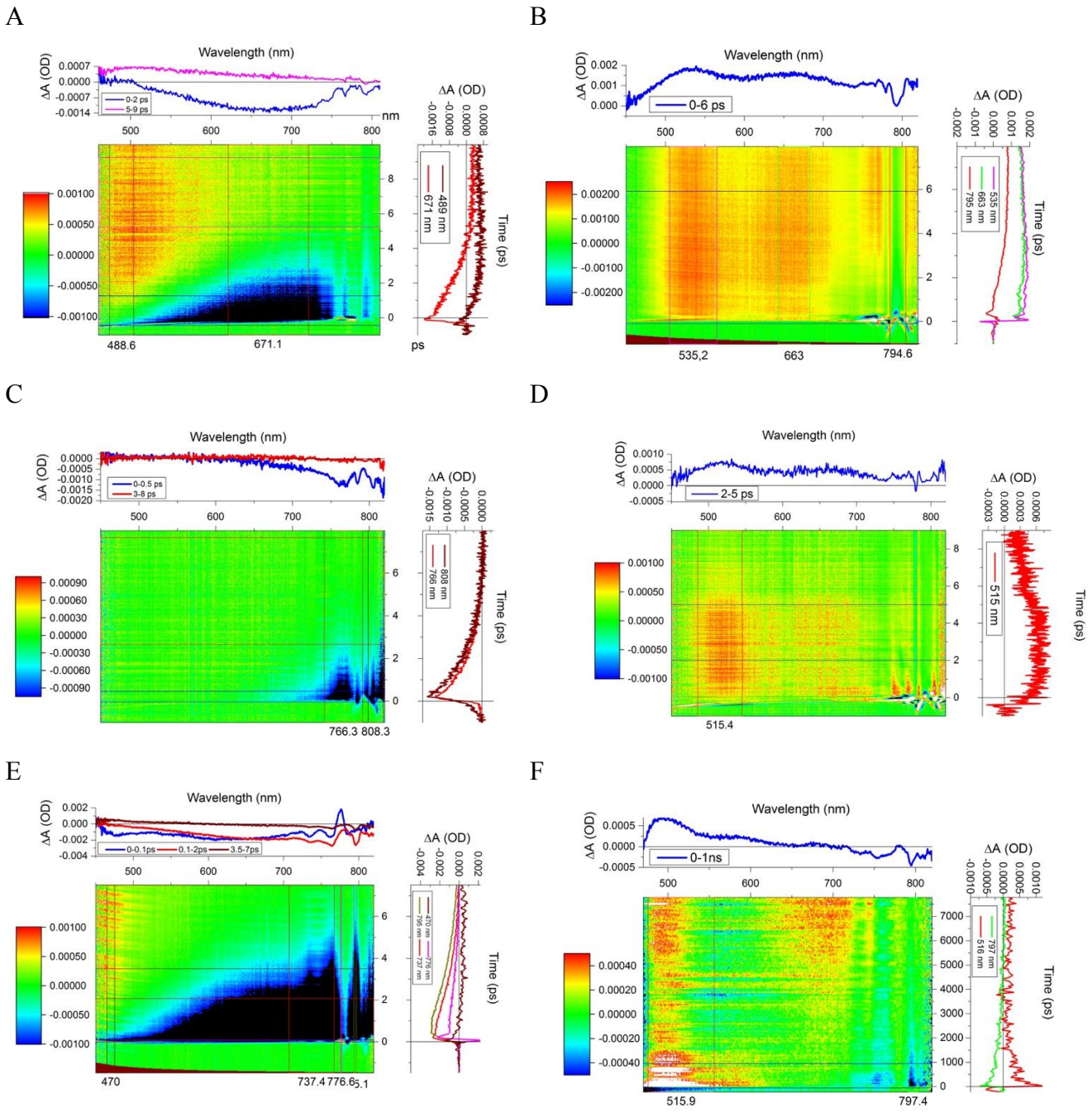

579 Figure 4

580

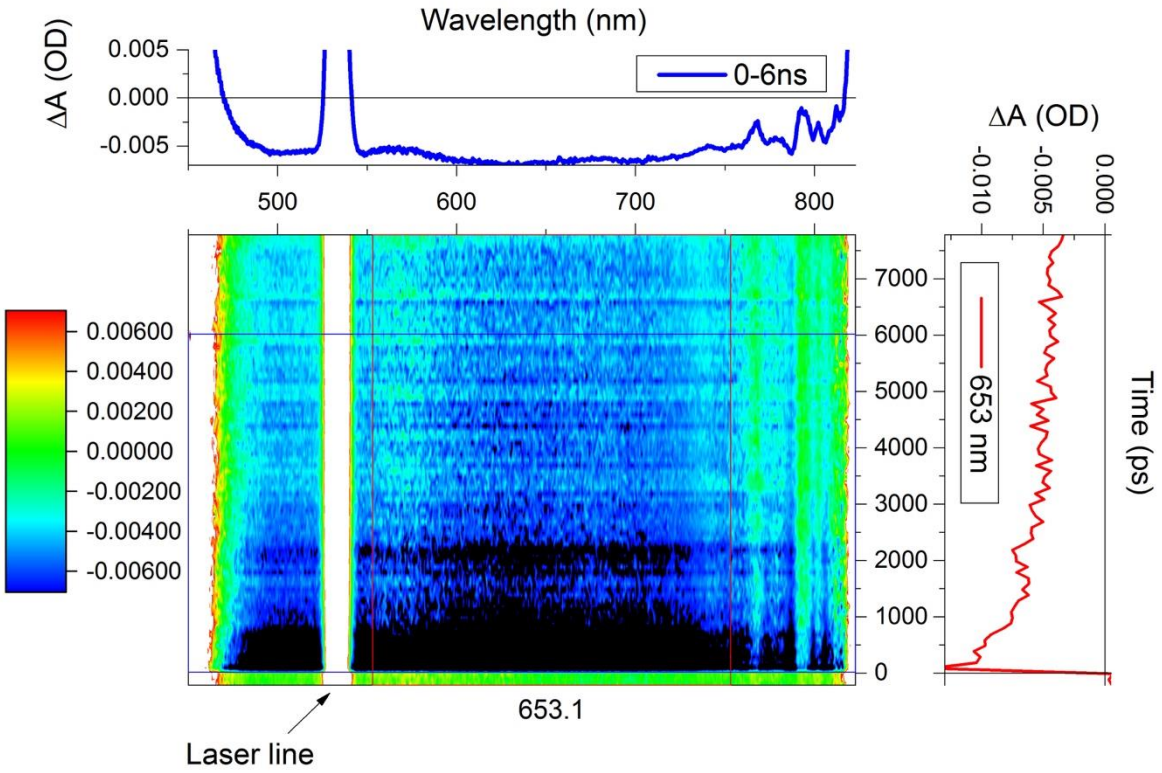

581
582 Figure 5

583
584

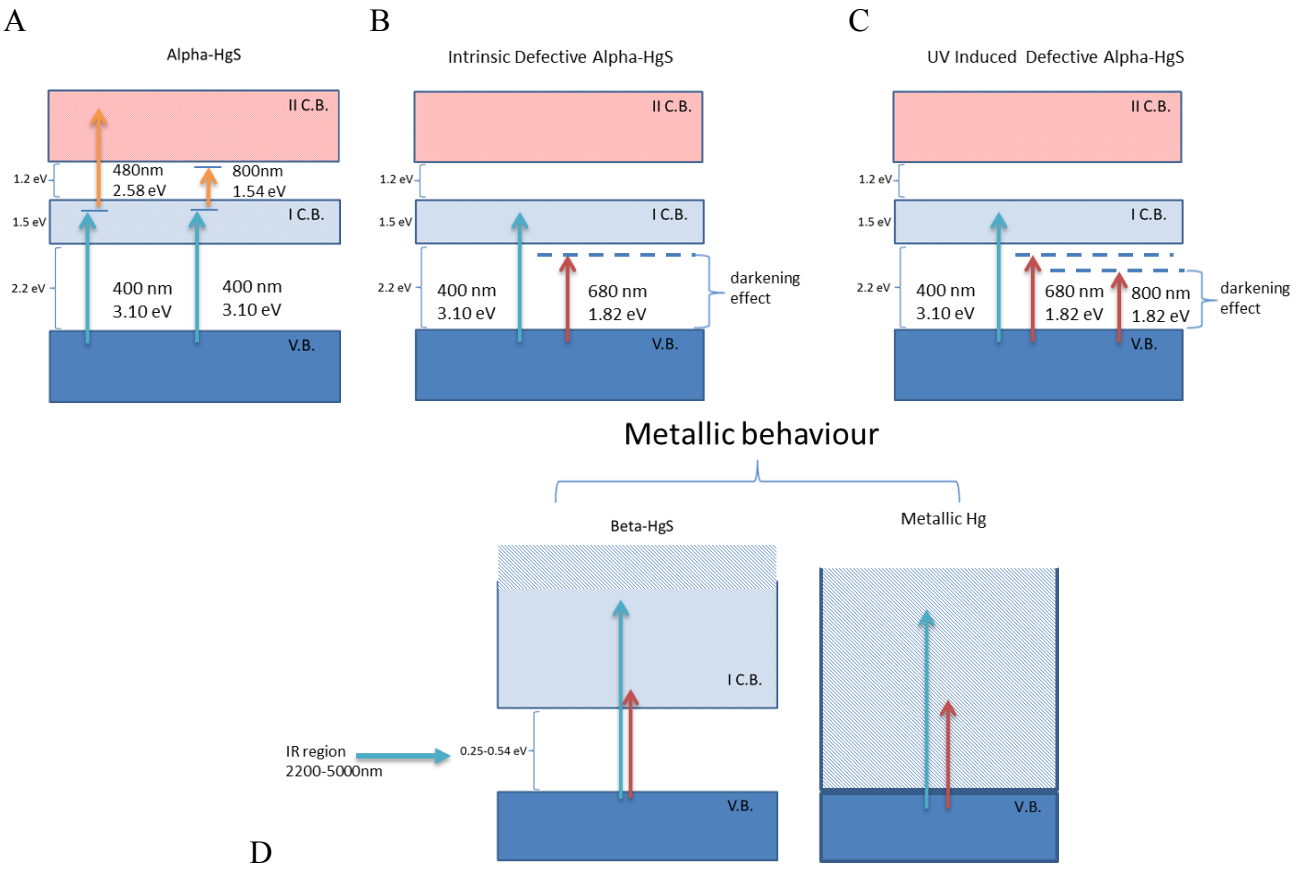

585
586 Figure 6
587

A

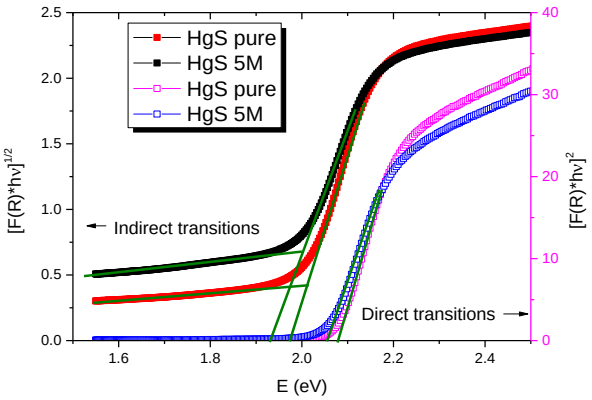

B

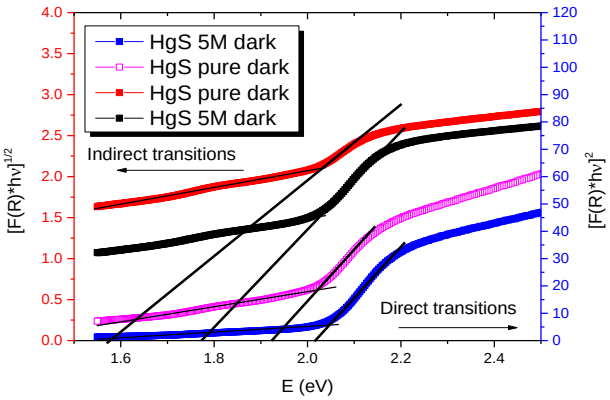

588 Figure 7
589

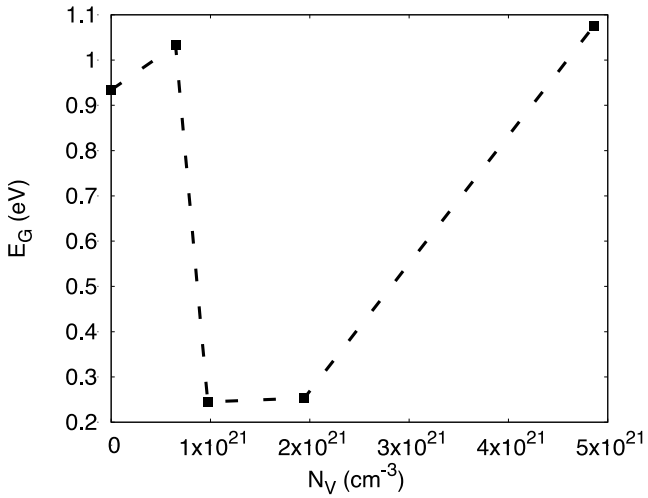
1.1
1
0.9
0.8
0.7
0.6
0.5
0.4
0.3
0.2
E_G (eV)
0
1x10^{21}
2x10^{21}
3x10^{21}
4x10^{21}
5x10^{21}
N_V (cm^{-3})

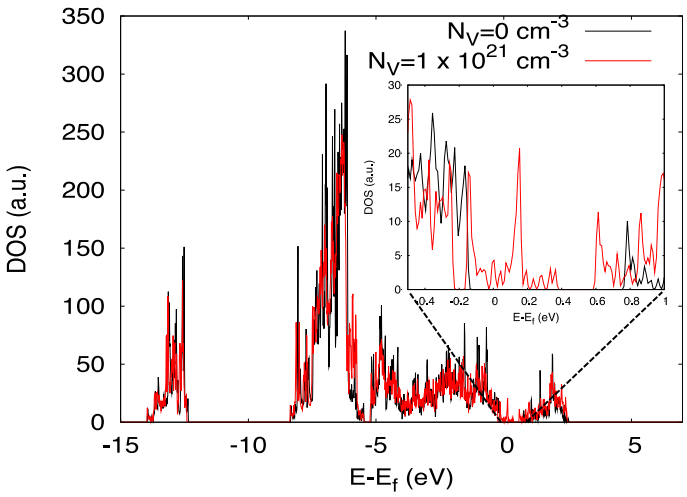
350
300
250
200
150
100
50
0
DOS (a.u.)
N_V=0 cm^{-3}
N_V=1 x 10^{21} cm^{-3}
-15
-10
-5
0
5
E-E_f (eV)
30
25
20
15
10
5
0
DOS (a.u.)
-0.4
-0.2
0
0.2
0.4
0.6
0.8
1
E-E_f (eV)

Figure 8

	(eV)	No UV	UV
Pure HgS	Direct transitions	2.05	1.92
	Indirect transitions	1.97	1.57
5M HgS	Direct transitions	2.08	2.01
	Indirect transitions	1.93	1.77

Table I